

Supporting Information

for

Net Negative Contributions of Free Electrons to the Thermal Conductivity of NbSe₃

Nanowires

Zhiliang Pan, †^a Lin Yang, †^a Yi Tao,^{a,b} Yanglin Zhu,^c Yaqiong Xu,^{d,e} Zhiqiang Mao,^c and Deyu

*Li^{*a}*

^aDepartment of Mechanical Engineering, Vanderbilt University, Nashville, TN 37235, USA.

^bSchool of Mechanical Engineering and Jiangsu Key Laboratory for Design and Manufacture of Micro-Nano Biomedical Instruments, Southeast University, Nanjing, 210096, P. R. China.

^cDepartment of Physics, Pennsylvania State University, University Park, PA 16802, USA.

^dDepartment of Electrical Engineering and Computer Science, Vanderbilt University, Nashville, TN 37235, USA.

^eDepartment of Physics and Astronomy, Vanderbilt University, Nashville, TN 37235, USA.

†: These authors contributed equally to this work

*: Author to whom correspondence should be addressed

E-mails: deyu.li@vanderbilt.edu

I. Extraction of Thermal Conductivity with a Depinning Electrical Field

For thermal measurement with the depinning electrical field applied across the nanowire, there is an electrical current passing through sample, which leads to Joule heating inside the nanowire. In addition, heat transfer associated with Peltier effect will also occur. We have considered these two effects in deriving the thermal conductance from raw data.

The schematic of the measurement system is shown in Figure S1. Here Joule heat from different components upon applying a depinning voltage to the sample is denoted as Q_{Rc1} , Q_{Rc2} , Q_w , Q_{b1} and Q_{b2} . Q_{Rc1} and Q_{Rc2} are due to the contact electrical resistance at nanowire-electrode junctions. Q_w is heat generation inside the nanowire. Q_{b1} and Q_{b2} are Joule heat generated by the platinum (Pt) lines connecting to the contact pads on the substrate. In addition, one more factor that must be considered is the Peltier cooling with the applied DC current across the sample, which move heat Q_p from one end to the other. T_h and T_s are the measured temperature rise of the heating and sensing membranes, respectively.

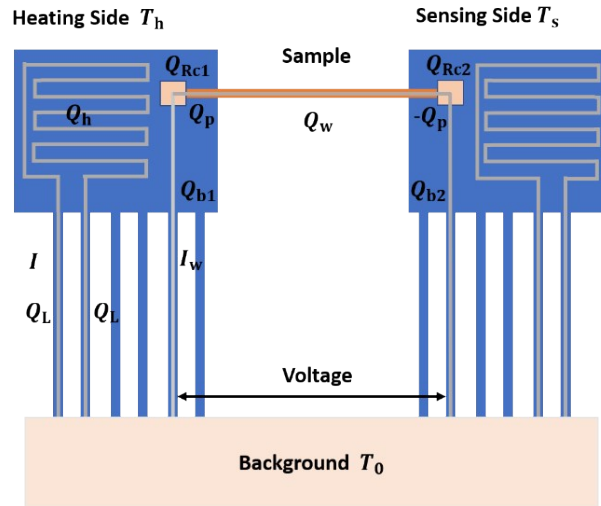


Figure S1. Schematic diagram of the measurement set-up.

These heat sources/sinks, together with the Joule heat on the heating side Q_h , and the two current carrying beams Q_L , can be expressed as

$$Q_h = I^2 \cdot R_h, \quad (S1)$$

$$2Q_L = 2I^2 \cdot R_L, \quad (S2)$$

$$Q_w = I_w^2 \cdot R_w, \quad (S3)$$

$$\begin{cases} Q_{b1} = I_w^2 R_{L1} \\ Q_{b2} = I_w^2 R_{L2}, \end{cases} \quad (S4)$$

$$\begin{cases} Q_{Rc1} = I_w^2 R_{c1} \\ Q_{Rc2} = I_w^2 R_{c2}, \end{cases} \quad (S5)$$

$$Q_p = \Pi_{ab} I = |S_{ab}| \Delta T I_w. \quad (S6)$$

Here I denotes the DC current passing through the serpentine Pt heating coil; and I_w denotes the DC current passing through the nanowire as a result of the applied depinning electric field. R_h , R_L , R_w and R_c represent the electrical resistance of the heating coil, the suspended leg/beam, the nanowire sample and the contact resistance, separately. Π_{ab} and S_{ab} are the Peltier coefficient and Seebeck coefficient between our sample and Pt probes. ΔT is the temperature difference between the two junctions.

All the heat will eventually dissipate to the substrate through the suspended legs/beams. We define Q_1 as the heat transferred to the substrate from the heating side, and Q_2 the heat transferred from sensing side.

Based on the energy conservation, we have

$$Q_1 + Q_2 = Q_h + 2Q_L + Q_w + Q_{Rc1} + Q_{Rc2} + Q_{b1} + Q_{b2}. \quad (S7)$$

For the two current carrying beams on the heating side, the heat diffusion equation can be written as

$$\frac{G_b L_b d^2 T}{6 dx^2} + \frac{Q_L}{L_b} = 0, \quad (\text{S8})$$

where G_b is the total thermal conductance of the six supporting beams. The boundary conditions to solve this equation are

$$T = T_h, x = 0 \text{ (on the heating membrane side)},$$

$$T = T_0, x = L_b \text{ (on the substrate side)}.$$

Here L_b is the length of support beams. Solving Eq. 8 with the given boundary conditions leads to the following temperature profile

$$T = T_h - \frac{3Q_L}{G_b L_b^2} x^2 + \left(\frac{3Q_L}{G_b L_b} - \frac{\Delta T_h}{L_b} \right) x. \quad (\text{S9})$$

Here $\Delta T_h = T_h - T_0$. The heat transfer from these two current-carrying beams is then

$$Q_{1,a} = 2 \times \frac{-G_b L_b}{6} \cdot \left(\frac{dT}{dx} \right)_{x=L_b} = \frac{G_b \Delta T_h}{3} + Q_L.$$

For the beam with I_w passing through it on the heating side, we have

$$\frac{G_b L_b d^2 T}{6 dx^2} + \frac{Q_b}{L_b} = 0. \quad (\text{S10})$$

The boundary conditions are

$$T = T_h, x = 0 \text{ (on the heating membrane side)},$$

$$T = T_0, x = L_b \text{ (on the substrate side)}.$$

Solving this equation, we get the temperature profile below

$$T = T_h - \frac{3Q_{b1}}{G_b L_b^2} x^2 + \left(\frac{3Q_{b1}}{G_b L_b} - \frac{T_h - T_0}{L_b} \right) x \quad (S11)$$

The heat transfer through this beam to the substrate is then

$$Q_{1,b} = \frac{-G_b L_b}{6} \cdot \left(\frac{dT}{dx} \right)_{x=L_b} = \frac{G_b \Delta T_h}{6} + \frac{1}{2} Q_b$$

The heat transferred through the other 3 beams without electrical current to the substrate can be expressed as

$$Q_{1,c} = \frac{G_b \Delta T_h}{2}$$

Sum all heat transfer from the heating membrane to the substrate, we have

$$Q_1 = Q_{1,a} + Q_{1,b} + Q_{1,c} = G_b \Delta T_h + Q_L + \frac{1}{2} Q_{b1} \quad (S12)$$

The sample itself is also under uniform Joule heating and the temperature is governed by

$$G_s L_s \frac{d^2 T}{dx^2} + \frac{Q_w}{L_s} = 0 \quad (S13)$$

The boundary conditions are

$$T = T_h, x = 0 \text{ (on the heating membrane side),}$$

$$T = T_s, x = L_s \text{ (on the sensing membrane side).}$$

The temperature profile along the sample is then

$$T = T_h - \frac{Q_w}{2G_s L_s^2} x^2 + \left(\frac{Q_w}{2G_s L_s} - \frac{\Delta T_h - \Delta T_s}{L_s} \right) x, \quad (S14)$$

where $\Delta T_s = T_s - T_0$. The heat transfer through sample to the sensing side is then $G_s(\Delta T_h - \Delta T_s) + Q_w/2$.

To conserve energy, the heat transfer from the sensing side to the substrate must be equal to the heat coming into the sensing membrane and the heat generated on the sensing membrane. So that

$$Q_2 = G_b \Delta T_s + \frac{1}{2} Q_{b2} = G_s (\Delta T_h - \Delta T_s) + \frac{Q_w}{2} + Q_{b2} + Q_{Rc2} - Q_p. \quad (\text{S15})$$

Combine Eqs. S7, S12 and S15, we can get

$$G_b = \frac{Q_h + Q_L + Q_w + (Q_{b1} + Q_{b2})/2 + Q_{Rc1} + Q_{Rc2}}{\Delta T_h + \Delta T_s}. \quad (\text{S16})$$

From Eq. S15 we have

$$G_s = \frac{G_b \Delta T_s - \frac{Q_w}{2} - \frac{Q_{b2}}{2} - Q_{Rc2} + Q_p}{\Delta T_h - \Delta T_s}. \quad (\text{S17})$$

In view that we are not able to get accurate values for the contact electrical resistance, Q_{Rc1} and Q_{Rc2} , the above equations cannot be used to solve for G_b and G_s . Fortunately, the expressions for G_b and G_s can be simplified to get rid of the unknown resistance. The heating comes from three sources, namely, Joule heat from the DC current to raise the temperature of the heating membrane, Joule heat generated by the depinning current, and Peltier effect that moves Q_p from one membrane to the other. The last two are induced by I_w and will be grouped together as the depinning component.

We split the temperature rise of the heating and sensing membranes into two components

$$\Delta T_h = \Delta T_{h,depin} + \Delta T_{h,IDC},$$

$$\Delta T_s = \Delta T_{s,depin} + \Delta T_{s,IDC}$$

Then we can rewrite Equation S16 and S17 into

$$G_b = \frac{Q_h + Q_L + Q_w + (Q_{b1} + Q_{b2})/2 + Q_{Rc1} + Q_{Rc2}}{\Delta T_h + \Delta T_s} = \frac{(Q_h + Q_L) + [Q_w + (Q_{b1} + Q_{b2})/2 + Q_{Rc1} + Q_{Rc2}]}{(\Delta T_{h,IDC} + \Delta T_{s,IDC}) + (\Delta T_{h,depin} + \Delta T_{s,depin})} \quad (S18)$$

$$G_s = \frac{G_b \Delta T_{s,IDC} + \left(G_b \Delta T_{s,depin} - \frac{Q_w}{2} - \frac{Q_{b2}}{2} - Q_{Rc2} + Q_p \right)}{(\Delta T_{h,IDC} - \Delta T_{s,IDC}) + (\Delta T_{h,depin} - \Delta T_{s,depin})} \quad (S19)$$

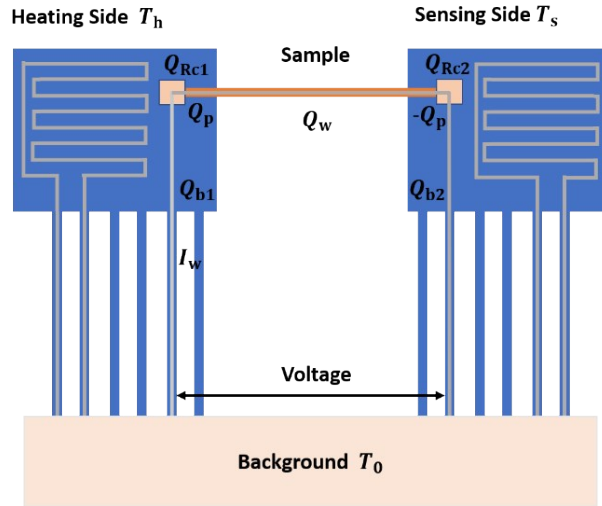


Figure S2. Schematic diagram demonstrating the effect of the depinning current.

In the experiment, if we only apply the depinning current without the DC heating current I_{DC} , as shown in Figure S2, the heating effect is only caused by the depinning current. In this case, the heat transferred from the heating side to the substrate is

$$Q_{1,depin} = G_b \Delta T_{h,depin} + \frac{1}{2} Q_{b1} \quad (S20)$$

Similarly, the heat transferred from the sensing side to the substrate is

$$Q_{2,depin} = G_b \Delta T_{s,depin} + \frac{1}{2} Q_{b2} \quad (S21)$$

Considering energy balance, we have

$$Q_{1,depin} + Q_{2,depin} = Q_{b1} + Q_{b2} + Q_{Rc1} + Q_{Rc2} + Q_w \quad (S22)$$

Combining Eqs. S20, S21 and S22, we obtain an expression for G_b as

$$G_b = \frac{Q_w + \frac{Q_{b1} + Q_{b2}}{2} + Q_{Rc1} + Q_{Rc2}}{\Delta T_{h,depin} + \Delta T_{s,depin}} \quad (S23)$$

In addition, the heat transfer from the heating side to the sensing side through the nanowire can be expressed as

$$Q_s = \frac{Q_w}{2} + G_s (\Delta T_{h,depin} - \Delta T_{s,depin}) - Q_p \quad (S24)$$

For the sensing side, we have

$$Q_{2,depin} = Q_s + Q_{b2} + Q_{Rc2} \quad (S25)$$

Combining Eqs S21, S24 and S25, we get

$$G_s = \frac{G_b \Delta T_{s,depin} - \frac{Q_w}{2} - \frac{Q_{b2}}{2} - Q_{Rc2} + Q_p}{\Delta T_{h,depin} - \Delta T_{s,depin}} \quad (S26)$$

Comparing Eqs. S18, S19, S24 and S26, mathematically we have

$$G_b = \frac{(Q_h + Q_L) + \left[Q_w + \frac{Q_{b1} + Q_{b2}}{2} + Q_{Rc1} + Q_{Rc2} \right]}{(\Delta T_{h,IDC} + \Delta T_{s,IDC}) + (\Delta T_{h,depin} + \Delta T_{s,depin})} = \frac{Q_w + \frac{Q_{b1} + Q_{b2}}{2} + Q_{Rc1} + Q_{Rc2}}{\Delta T_{h,depin} + \Delta T_{s,depin}} = \frac{Q_h + Q_L}{\Delta T_{h,IDC} + \Delta T_{s,IDC}}, \quad (S27)$$

$$G_s = \frac{G_b \Delta T_{s,IDC} + \left(G_b \Delta T_{s,depin} - \frac{Q_w}{2} - \frac{Q_{b2}}{2} - Q_{Rc2} + Q_p \right)}{(\Delta T_{h,IDC} - \Delta T_{s,IDC}) + (\Delta T_{h,depin} - \Delta T_{s,depin})} = \frac{G_b \Delta T_s - \frac{Q_w}{2} - \frac{Q_{b2}}{2} - Q_{Rc2} + Q_p}{\Delta T_h - \Delta T_s} = \frac{G_b \Delta T_{s,IDC}}{\Delta T_{h,IDC} - \Delta T_{s,IDC}}. \quad (\text{S28})$$

The above two equations allow us to extract the thermal conductance of the supporting legs/beams and the nanowire sample with an applied depinning electric field. The essential idea is that the heating effects of the depinning voltage are a background that can be canceled out in the derivation of the beam and wire conductance.

II. Contact Treatment to Minimize the Electrical and Thermal Resistance

Our measurement indicates that the electrical resistance at the two contacts between the nanowire sample and suspended membranes without any treatment can be over 100 k Ω at 50 K. While this value only has marginal effect on the derived electrical conductance as we use the four-probe method to measure it. The large contact electrical resistance does affect the thermal measurement under the depinning condition as the contact resistance can induce a temperature rise of more than 50 K with the applied depinning voltage. To minimize this temperature rise, it is critical to reduce the contact electrical resistance. To do so, we fine tune our electron-beam induced deposition process based on published reports¹⁻⁴ by selecting a larger operating current of 1.4 nA to increase the content of Pt in the deposited Pt/C mixture to achieve a low the contact resistance. The measured contact electrical resistance is shown in Figure S3, which shows that it is reduced to be below 1 k Ω . Doing so, the overall temperature rise is measured to be less than 6 K during the thermal measurement.

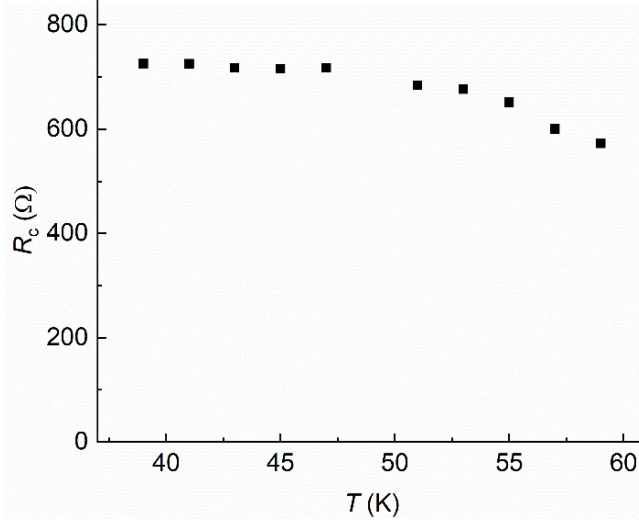


Figure S3. The measured contact electrical resistance versus temperature.

III. Effects of Drift Velocity

The strongest electric field we applied for depinning is below 2 V/cm. Based on the mobility of electrons in NbSe₃,⁵ the maximum drift velocity is calculated as

$$v_d = \mu E = 1500 \text{ cm}^2/(\text{V} \cdot \text{s}) \times 2 \text{ V/cm} = 3 \times 10^3 \text{ cm/s}. \quad (\text{S29})$$

The Fermi velocity v_F in NbSe₃ is estimated to be $2.5 \times 10^7 \text{ cm/s}$.⁶ Therefore, the drift velocity is less than 0.02% of the Fermi velocity and the contribution of the external electric field to the electronic thermal conduction can be neglected.

IV. Scattering Rates due to Different Scattering Mechanisms

Phonon mode dependent scattering rates and phonon mean free path (MFP) from different scattering mechanisms is provided at 47 K. As shown in Figure S4a, the phonon-phonon (ph-ph) scattering plays a minor role (the scattering rate is only in gigahertz regime across the entire spectrum) at this low temperature regime (47 K). In contrast, electron-phonon (e-ph), phonon-boundary and phonon-impurity scattering all make appreciable contributions to the total phonon scattering rate. It is shown that boundary scattering is more important for low frequency phonons

while e-ph scattering and defect scattering play important roles across the entire spectrum. Under depinning conditions, e-ph scattering rate further increases due to the enhanced free electron concentration, which suggests that the reduction in lattice thermal conductivity is indeed due to the enhanced e-ph scattering rate. Similar conclusions can also be drawn from the corresponding MFP in Figure S4b.

We note that while usually e-ph scattering is only important in high temperature region for electrical transport, it can play a critical role for phonon transport at low temperatures as ph-ph scattering is also drastically suppressed as temperature drops.

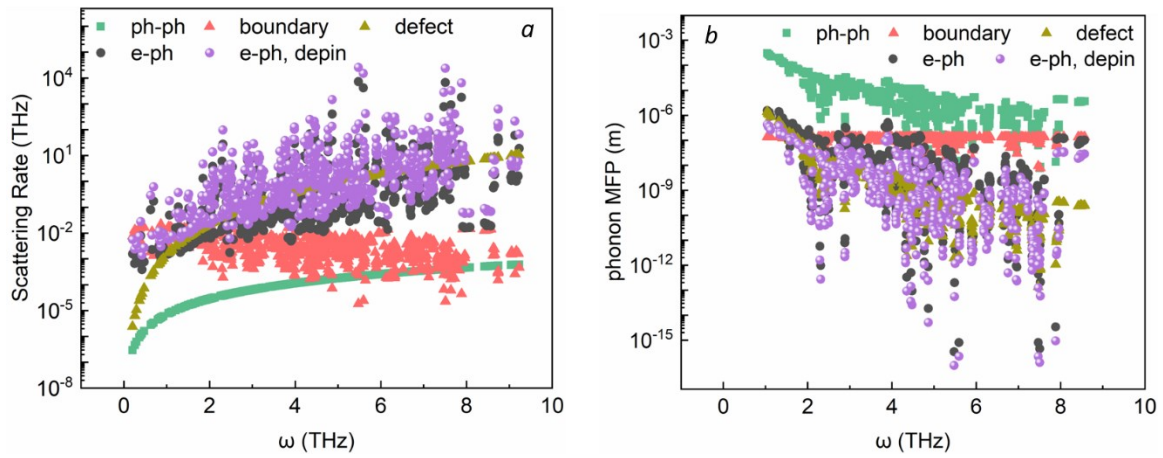


Figure S4. (a) Scattering rates of different mechanisms at 47 K; (b) Phonon MFP determined by different mechanisms at 47 K.

V. Effects of the Depinning Current on Lattice Thermal Conductivity

We plotted the lattice thermal conductivity as a function of the electrical current in Figure S5a for a 94 nm diameter wire. It can be seen that the lattice thermal conductivity continuously decreases with the increasing depinning current before it reaches $\sim 5.5 \mu\text{A}$, beyond which the lattice thermal conductivity stays the same as no more condensed electrons are depinned.

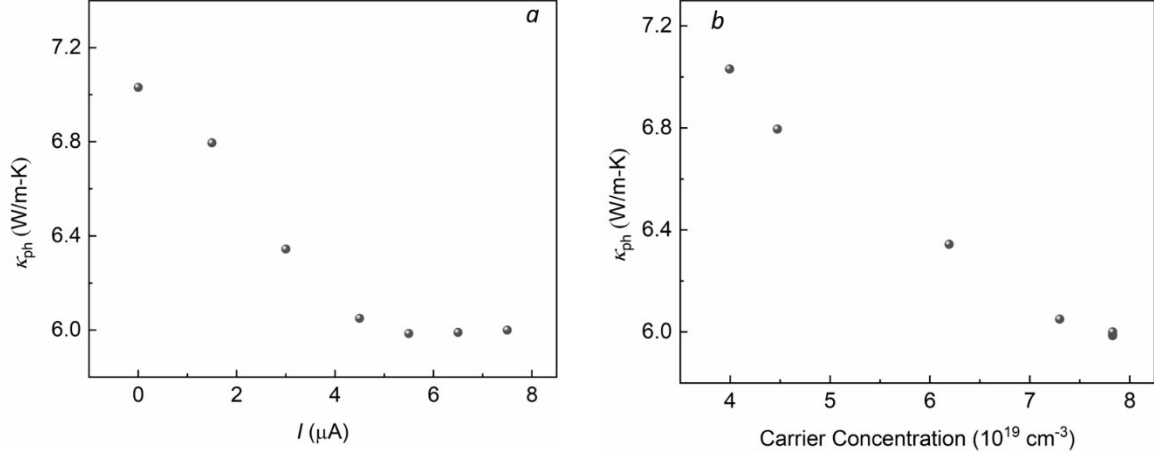


Figure S5. Lattice thermal conductivity as a function of (a) the depinning current, and (b) the carrier concentration, during depinning test for the 94 nm NbSe₃ nanowire sample at 47 K.

Figure S5b shows the relation between the carrier concentration and lattice thermal conductivity, which shows that increased electron concentration leads to a stronger e-ph scattering and thus a reduced lattice thermal conductivity. This plot further demonstrates the reduction in lattice thermal conductivity is induced carrier concentration variation, not depinning current and other factors.

VI. Uncertainty Analysis

The derived thermal conductivity tolerates noises from the thermal conductance uncertainty, and uncertainties associated with the length and cross-sectional area measurement. Based on the formula below

$$\kappa = \frac{GL}{A}, \quad (\text{S30})$$

where G is the measured thermal conductance, L is the measured length of the nanowire, and A is cross section area, the uncertainty of thermal conductivity can be estimated as

$$\frac{\delta\kappa}{\kappa} = \sqrt{\left(\frac{\delta G}{G}\right)^2 + \left(\frac{\delta L}{L}\right)^2 + \left(\frac{\delta A}{A}\right)^2}. \quad (\text{S31})$$

The uncertainty of thermal conductance is estimated to be 2 ~ 3% depending on temperature using a Monte Carlo simulation approach in our previous work.⁷ The length L is measured by SEM, and the uncertainty is evaluated as 0.2 μm , which introduce about 3% uncertainty for our ~6.5 μm long sample. The relative uncertainty for the cross-sectional area is conservatively estimated to be 10%. Together, the overall uncertainty for the derived thermal conductivity is determined to be 11% at 300 K.

The electrical resistance of our samples was calculated by taking the slope of the linear fitted I-V curve. The uncertainty is calculated by

$$U_R = \sqrt{\frac{\sum (V_i - RI_i - b)^2}{n-2}} \times \frac{n}{n \sum I_i^2 - (\sum I_i)^2}, \quad (\text{S32})$$

where n is the number of measured data points, b is the fitted intercept representing zero-point current shift. U_R is calculated to be 5.4 Ω at 300 K for our 94 nm diameter sample. This is only 0.47 % of the linear fitted resistance (1148.8 Ω). As such, we didn't show the error bar for electrical resistance in the main paper.

REFERENCES

1. W. F. Van Dorp, C. W. Hagen, *J. Appl. Phys.* 2008, **104**, 081301.
2. M. Weber, H. W. P. Koops, M. Rudolph, J. Kretz, G. Schmidt, *J. Vac. Sci. Technol. B* 1995, **13**, 1364–1368.
3. Y. M. Lau, P. C. Chee, J. T. L. Thong, V. Ng, *J. Vac. Sci. Technol. A*, 2002, **20**, 1295–1302.
4. M. Weber, M. Rudolph, J. Kretz, H. W. P. Koops, *J. Vac. Sci. Technol. B*, 1995, **13**, 461–464.

5. N. P. Ong, *Phys. Rev. B*, 1978, **18**, 5272–5279.

6. J. McCarten, D. A. DiCarlo, M. P. Maher, T. L. Adelman, E. Thorne, *Phys. Rev. B*, 1992, **46**.

7. J. Yang, Y. Yang, S. W. Waltermire, T. Gutu, A. A. Zinn, T. T. Xu, Y. Chen, D. Li, *Small* 2011, **7**, 2334–2340.